Fast Spherical Harmonic Analysis: a quick algorithm for generating and/or inverting full sky, high resolution CMB Anisotropy maps

Pio Francesco Muciaccia
Dipartimento di Fisica, Università di Roma,"Tor Vergata"
Via della Ricerca Scientifica, 00133 Roma, Italy

Paolo Natoli
Dipartimento di Fisica, Università di Roma, "Tor Vergata"
Via della Ricerca Scientifica, 00133 Roma, Italy

Nicola Vittorio
Dipartimento di Fisica, Università di Roma, "Tor Vergata"
Via della Ricerca Scientifica, 00133 Roma, Italy

Abstract

We present a fast algorithm for generating full sky, high resolution ($\sim 5'$) simulations of the CMB anisotropy pattern. We also discuss the inverse problem, that of evaluating from such a map the full set of $a_{\ell m}$'s and the spectral coefficients C_ℓ. We show that using an Equidistant Cylindrical Projection of the sky substantially speeds up the calculations. Thus, generating and/or inverting a full sky, high resolution map can be easily achieved with present day computer technology.

Subject Headings: cosmic microwave background

1 Introduction

The angular power spectrum of CMB anisotropies is a gold-mine of cosmological information. It sensitively depends upon a number of parameters: the total and baryonic density parameters, Ω_0 and Ω_b; the cosmological constant, Λ; the Hubble constant, H_0; the spectral indices, n_s and n_t , and the amplitudes of scalar and tensor metric fluctuations; the redshift, z_{rh} , at which the universe could have been reionized. Because of their planned high sensitivity and high angular resolution, future space missions will measure the anisotropy power spectrum with great accuracy. Thus, all these cosmological parameters will be determined with an unprecedented precision (Bersanelli *et al.* 1996; Jungman *et al.* 1996)

To achieve these goals, Monte Carlo simulations of the CMB anisotropy pattern have been and will be more and more crucial in this game. From one hand, they allow to prepare a mission, to optimize the observational strategy and to test for different payload configurations. On the other hand, they are important for the data analysis and, for example, to look for systematics.

Up to now, these simulations were realized without problems. Experiments with high angular resolution observed only very limited region of the sky: FFT techniques easily provided several realizations of small (and, hence, flat) patches of the sky (see *e.g.* Kogut, Hinshaw and Bennett, 1995). Experiments with large sky coverage, such as COBE/DMR, had low resolution: several full sky, CMB anisotropy maps were easily generated through a spherical harmonic expansion with a low ($\lesssim 100$) number of harmonics.

A potential problem it is claimed to arise in generating even a single high resolution, full sky map (see, *e.g.* Saez, Holtmann and Smoot, 1996), too much, it is believed, for present computer technology. It is generally perceived as a heavy, almost impossible, computational task also the inverse problem, that is extracting out of an observed full sky, high resolution map the anisotropy spectrum up to $\ell \gtrsim 1000$. In fact, to our knowledge, anisotropy spectrum estimates have always been done applying FFT techniques either to small patches of , or even to the whole (FFT simulated) sky. The latter approach is in principle wrong and its accuracy has still to be checked for.

The purpose of this paper is quite technical, but of interest, we believe, to the large community involved in future CMB anisotropy experiments. We want to present a fast algorithm for: i) generating high resolution ($\lesssim 10'$), full sky maps; ii) reconstructing all the coefficients of a spherical harmonic expansion, and hence the spectral coefficient C_ℓ, up to $\ell \gtrsim 1000$. Both these tasks can be easily achieved on currently available workstations. Thus, the plane of this Letter is as follows. In Sect.2 we will describe the method. In Sect.3 we will discuss numerical results and the efficiency of the method. Finally in Sect.4 we will present a brief summary of our main findings.

2 Method

Generating a CMB anisotropy map is in principle very simple. The temperature fluctuation observed along a line of sight, $\hat{\gamma}$, can be conveniently described by a spherical harmonic expansions:

$$\frac{\Delta T}{T}(\vec{x},\hat{\gamma}) = \sum_{\ell=0}^{\ell_{max}} \sum_{m=-\ell}^{\ell} a_{\ell m}(\vec{x}) Y_{\ell m}(\hat{\gamma}) \tag{1}$$

where $a_{\ell,-m} = (-1)^m a^*_{\ell m}$. The $a_{\ell m}$'s are random variables of the observer position, $\vec{x}$, gaussian distributed (at least in most of the inflation based scenarios), with zero mean and variances $\langle |a_{\ell m}|^2 \rangle \equiv C_\ell$. In simulating the CMB, primary anisotropy pattern the sum over ℓ usually starts from two. In fact, from one hand the monopole vanishes by construction, being the mean (over the sky) CMB anisotropy. On the other hand, the dipole components are dominated by the Doppler anisotropy, induced by our peculiar motion relative to the comoving frame (see *e.g.* Kogut *et al.* 1994). On the same line, we will keep the sum over ℓ from 0 to ℓ_{max}, but we set $a_{00} = a_{1,-1} = a_{1,0} = a_{1,1} = 0$.

The C_ℓ's are the main prediction of a theory of structure formation (see *e.g.* Hu and Sugiyama, 1996). Thus, for a given scenario (*i.e.* for given C_ℓ's) and for a given statistics, we can generate a random set of $a_{\ell m}$'s and, from Eq.(1), a CMB anisotropy map. In practice, using the spherical harmonic expansion as in Eq.(1) is not very efficient: for each line of sight $\hat{\gamma}$ we should evaluate $Y_{\ell m}(\hat{\gamma})$ for each value of ℓ and m. Fortunately, it is possible to rewrite Eq.(1) in a form more suitable for numerical implementation.

First, it is easy to verify that the double sum in Eq.(1), $\sum_{l=l_0}^{l=l_{max}} \sum_{m=-\ell}^{m=+\ell}$, is completely equivalent to $\sum_{m=-\ell_{max}}^{m=+\ell_{max}} \sum_{\ell=|m|}^{\ell=\ell_{max}}$: we sample exactly the same region of the $\ell - m$ space, by columns (in the former) or by rows (in the latter case; *c.f.* Fig.1). Second, let us write

$$Y_{\ell m}(\theta, \phi) = \lambda_\ell^m(\cos\theta) e^{im\phi}, \tag{2}$$

where

$$\lambda_\ell^m = \sqrt{\frac{2\ell+1}{4\pi}\frac{(\ell-m)!}{(\ell+m)!}} P_\ell^m(\cos\theta), \tag{3}$$

$\lambda_\ell^{-m} = (-)^m \lambda_\ell^m$ and $P_\ell^m(\cos\theta)$ are the associated Legendre polynomials. It is then possible to rewrite Eq.(1) as follows:

$$\frac{\Delta T}{T}(\phi, \theta) = \sum_{m=-\ell_{max}}^{m=+\ell_{max}} b_m(\theta) e^{im\phi} \tag{4}$$

where

$$b_m = \sum_{\ell=|m|}^{\ell=\ell_{max}} a_{\ell m} \lambda_\ell^m \tag{5}$$

and $b_{-m} = b_m^*$. Written in this way, Eq.(4) highlights a couple of attractive features. If we use an Equidistant Cylindrical Projection (hereafter ECP) of the sky, which conserves distances along meridians and along the equator, the anisotropy map can be thought as a rectangular matrix of N_ϕ times $N_\theta (= N_\phi/2)$ squared pixels, each of dimension $\simeq 20' \times 20'(1024/N_\phi)^2$. In this projection, the temperature anisotropy along parallels (*i.e.* at fixed θ) is nothing more than the 1D Fourier transform of the coefficients $b_m(\theta)$'s [*c.f.* Eq.(4)], very efficiently computed with FFT techniques. If we regard the sum of Eq.(4) as a Fourier expansion, then ℓ_{max} must be fixed to be $N_\phi/2$, as it plays the role of the Nyquist critical frequency of the problem. Second, the λ_ℓ^m are evaluated by standard recurrence relations:

$$\begin{aligned}
\lambda_m^m &= (-1)^m \sqrt{\frac{2m+1}{4\pi}} \frac{(2m-1)!!}{\sqrt{(2m)!}} (1-x^2)^{m/2} \\
\lambda_{m+1}^m &= x\sqrt{2m+3}\,\lambda_m^m \\
\lambda_\ell^m &= \left[x\lambda_{\ell-1}^m - \sqrt{\frac{(l+m-1)(l-m-1)}{(2\ell-3)(2\ell-1)}}\lambda_{\ell-2}^m\right] \sqrt{\frac{4\ell^2-1}{\ell^2-m^2}}
\end{aligned} \tag{6}$$

where $x = \cos\theta$. Because of these relations, the $b_m(\theta)$'s can be computed very efficiently, as we can perform the sum in Eq.(5) while computing the λ_ℓ^m's. Such a computation is further simplified because $\lambda_{\ell m}(\cos\theta) = \pm\lambda_{\ell m}[\cos(\pi - \theta)]$, the plus (minus) sign holding if ℓ and m are (are not) both even or both odd.

Generating the $b_m(\theta)$'s at fixed θ requires evaluating $\approx \ell_{max}^2$ ($\propto N_\phi^2$) recurrence relations ($\ell_{max} - m$ recurrence relations for each value of m). The CPU time needed for FFT-ing the $b_m(\theta)$'s in principle scales as $N_\phi \ln N_\phi$. However, the FFT is so fast that for $N_\phi \leq 4096$ most of the time is spent for generating the $b_m(\theta)$'s. Finally, we have to evaluate the $b_m(\theta)$'s N_θ times. So, at the end, the total CPU time needed for generating an ECP of the anisotropy pattern is expected to scale as N_ϕ^3.

At this point it is quite easy to address also the inverse problem, that of evaluating from an observed high resolution, full sky map the set of coefficients $a_{\ell m}$. It is very well known that the orthonormality of the spherical harmonics allows to invert Eq.(1) and write:

$$a_{\ell m} = \int d\Omega \frac{\Delta T}{T}(\hat{\gamma}) Y^*_{\ell m}(\hat{\gamma}) \tag{7}$$

This sounds awful: in principle for each ℓ and m we should evaluate $Y_{\ell m}(\hat{\gamma})$ for a given $\hat{\gamma}$ and integrate over the whole sky. Fortunately, after substituting Eq.(2) in Eq.(7) we can write:

$$a_{\ell m} = \int \sin\theta d\theta \lambda_\ell^m(\theta) b_m(\theta) \tag{8}$$

where

$$b_m(\theta) = \int_0^{2\pi} d\phi \Delta(\phi, \theta) \exp(-im\phi) \tag{9}$$

Thus, Eq.(8) is the conjugate of Eq.(4): the b_m's are the Fourier anti-transform of the anisotropy pattern along a parallel in the ECP of the sky, and are easily computed at fixed θ with a FFT. In conclusion, inverting a map to obtain the $a_{\ell m}$'s requires $\approx \ell_{max}^2$ ($\propto N_\phi^2$) recurrence relations for evaluating the λ_ℓ^m's, plus a FFT to evaluate the b_m's. All this must be done N_θ ($\propto N_\phi$) times to be able to perform the integral in Eq.(8). Using these tricks, we can invert a full sky, high resolution map with CPU times which scale as N_ϕ^3 (the evaluation of the $b_{\ell m}$'s is basically instantaneous), and in principle comparable with

those needed for generating a map. As in that case, the actual CPU time can be further reduced by exploiting the simmetries of the $\lambda_{\ell m}$'s evaluated at θ and $\pi - \theta$, respectively.

3 Numerical Results

In the previous Section we described an algorithm for generating and/or inverting a high resolution, full sky map of the CMB anisotropy. In this Section we will briefly discuss the actual performances of this algorithm on a DEC 1000/200. We will consider hereafter the standard Cold Dark Matter model.

In Fig.2 we plot the CPU time needed for generating a full sky, ECP of the CMB anisotropy pattern as a function of the angular resolution, the only free parameter we can play with. In fact, we sample the ECP of the sky with $N_\phi \times N_\theta$ squared pixels of dimension $20' \times 20'(1024/N_\phi)^2$. This fixes $N_\theta = \ell_{max} = N_\phi/2$. The expected scaling with N_ϕ^3 (see Sect.2) is recovered with good precision. We want to stress that only 1h of CPU time is needed to generate a full sky, ECP of the CMB anisotropy with a resolution of $5'$ (*i.e.* $N_\phi = 4096$).

Using an ECP is not a limitation. In fact, once we obtain an ECP of the anisotropy pattern, we can reproduce it in any given projection. As an example we show in Plate 1 an ECP, 10' resolution map (obtained in only 8 minutes of CPU time) and the corresponding Equal Area Projection (hereafter EAP). The latter is obtained by the former using standard spherical trigonometry. We verified that this procedure is numerically stable. In fact, if we transform an ECP to an EAP and the obtained EAP back to an ECP, we reproduce the initial anisotropy pattern exactly. Thus, from observations of the CMB anisotropy we can create an ECP of the sky and then apply our inversion algorithm. In Fig.2 we also show the CPU time needed for inverting an ECP map as a function of the map resolution. The CPU time scales roughly as N_ϕ^3. Again, $\simeq 1h$ of CPU time is needed to recover from a $5'$ resolution map the entire set of $a_{\ell m}$'s, roughly $4 \cdot 10^6$ coefficients.

In Figs.3 and 4 we show the precision of our inversion algorithm for $\ell_{max} = 1024$ (corresponding to a resolution of $10'$) . The percentage error between the recovered $a_{\ell m}$'s

and the input ones is large only for $\ell \sim \ell_{max}$ and $m \sim$ few, a very small portion of the allowed region of the $\ell - m$ space. This is due to the fact that for $m \to 0$, $\lambda_\ell^0 \propto P_\ell(\cos\theta)$: for large values of ℓ, this is a highly oscillating function of θ. On the contrary, for $m \to \ell$, $\lambda_\ell^\ell \propto (1-\cos\theta)^{\ell/2}$, a quite smooth function of the azimuthal angle [*c.f.* Eq.(6)]. So, a simple trapezoidal rule for performing the integral along meridians in Eq.(8) gives a poor result only for very large values of ℓ and quite small values of m. However, this is not a crucial problem. In fact, we are mostly interested in evaluating the spectral coefficients C_ℓ. These are obtained from the recovered $a_{\ell m}$'s as follows:

$$C_\ell^{estimated} = \frac{1}{2\ell+1} \sum_{m=-\ell}^{\ell} |a_{\ell m}|^2 \tag{10}$$

It is clear that the error we make in recovering the $a_{\ell m}$'s for large ℓ and small m is highly diluted in the sum of Eq.(10). In Fig.5 we show the (percentage) error between the recovered and the input C_ℓ's as a function, again, of the map resolution. The recovered spectrum has a maximum error of $\sim 0.1\%$ up to $\ell \lesssim 1500$ for $N_\phi = 4096$, *i.e.* for a pixel size of $5' \times 5'$.

4 Conclusions

We present a fast algorithm for: i) generating high resolution, full sky maps of the CMB anisotropy; ii) evaluating out of an observed map the $a_{\ell m}$'s and then the spectral coefficient C_ℓ's. The basic trick for speeding up the calculation consists in generating and/or inverting a full sky map using an ECP. It is this projection that allows the use of a FFT either in Eq.(4) and/or in Eq.(9). If we are interested in probing the anisotropy power spectrum up to $\ell_{max} \simeq 1000$, then $N_\phi = 2\ell_{max} = 2048$ and we need only 8 minutes of CPU time for either generating or inverting a $10'$ resolution, full sky map. Pushing the sampling down to $5'$ boosts the needed CPU time up to one hour. Our algorithm also allows us to fully exploit a parallel architecture, such as the one of APEmille (Bartoloni *et al.* 1995). This machine is composed by 1024 processors, each of them slower by roughly a factor of two w.r.t. a DEC 1000/200. So, with such a machine one should be able to produce

1024, $5'$ resolution maps of the anisotropy pattern in a couple of hours. Details about this application will be discussed elsewhere.

In addressing the problem of inverting a full sky map, we assumed full sky coverage and we fully exploited the orthonormality of the spherical harmonics. We test our algorithm against a pure CMB anisotropy pattern. In the realistic case, a μ-wave map will be the superposition of different processes (CMB anisotropy, Galactic foregrounds, secondary anisotropy due to clusters of galaxies, point sources, etc.) and the sky coverage can be not complete. The separation of the CMB anisotropy pattern from Galactic and extragalactic foregrounds has been studied in details (Bouchet *et al.* 1994; Bouchet *et al.* 1995; Bersanelli *et al.* 1996), but considering only small ($10^o \times 10^o$) patches of the sky. We will discuss an application of our algorithm to the problem of foreground subtraction and not complete sky coverage in a forthcoming paper.

References

[1] Bartoloni *et al.* 1995, *Nucl.Phys.B*,**42**,17

[2] Bersanelli, M. Bouchet, F.R., Efstathiou, G., Griffin, M., Lamarre, J.M., Mandolesi, N., Norgaard-Nielsen, H.U., Polny, J., Vittorio, N., Pace, O., Tauber, J., Volonte', S. 1996, *COBRAS/SAMBA Report on the Phase A Study*, ESA D/SCI(96)3

[3] Bouchet, F.R., Gispert, R., Puget, J.L. 1995, Proceedings of the Moriond Meeting on *Clustering in the Universe*, Editions Frontieres

[4] Bouchet, F.R., Gispert, R., N.Aghanim, Bond, J.R., de Luca, A., Hivon, E. and Maffei, B. 1994, in Proceedings of the Meeting on *Far Infrared and Sub-millimeter Space Missions in the Next Decade*, Space Scinece Review, Eds. Sauvage M.

[5] Hu,W. and Sugiyama, N. 1995,Phys.Rev., D51,2599

[6] Jungman, G., Kamionkowski, M., Kosowski, A. & Spergel, D.N., astro-ph/9512139

[7] Kogut, A. *et al.* 1994, *Ap.J.Lett.* ,**419**,L5

[8] Kogut, A. Hinshaw, G. and Bennett, C.L. 1995, *Ap.J.Lett.*, **441**,L5

[9] Saez, D., Holtmann, E., Smoot, G.F. 1996, astro-ph/9606164

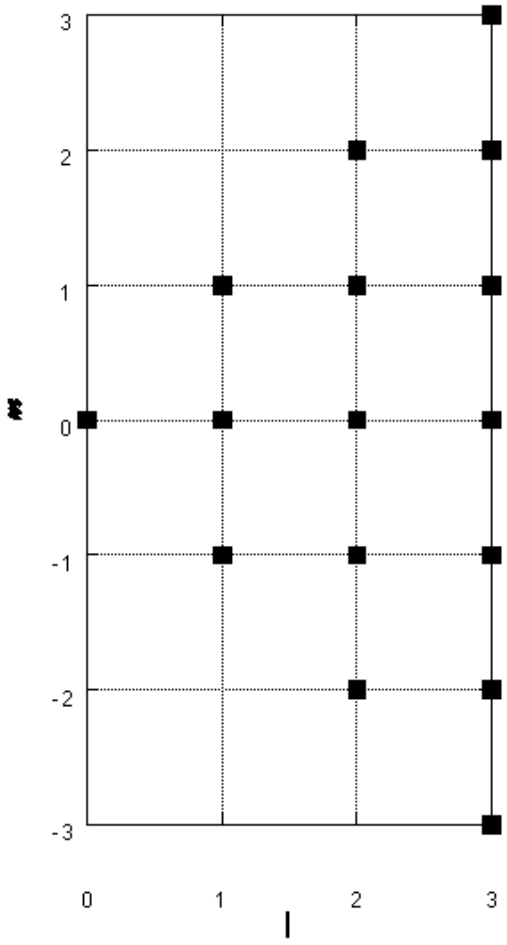

Figure 1: The filled squares show (for $\ell_{max} = 3$) the portion of the $\ell - m$ space probed by the $a_{\ell m}$'s. We can recover all the allowed $\ell - m$ pairs either by moving along columns ($\sum_{\ell=0}^{\ell_{max}} \sum_{m=-\ell}^{\ell}$) or by rows ($\sum_{m=-\ell_{max}}^{m=+\ell_{max}} \sum_{\ell=|m|}^{\ell=\ell_{max}}$).

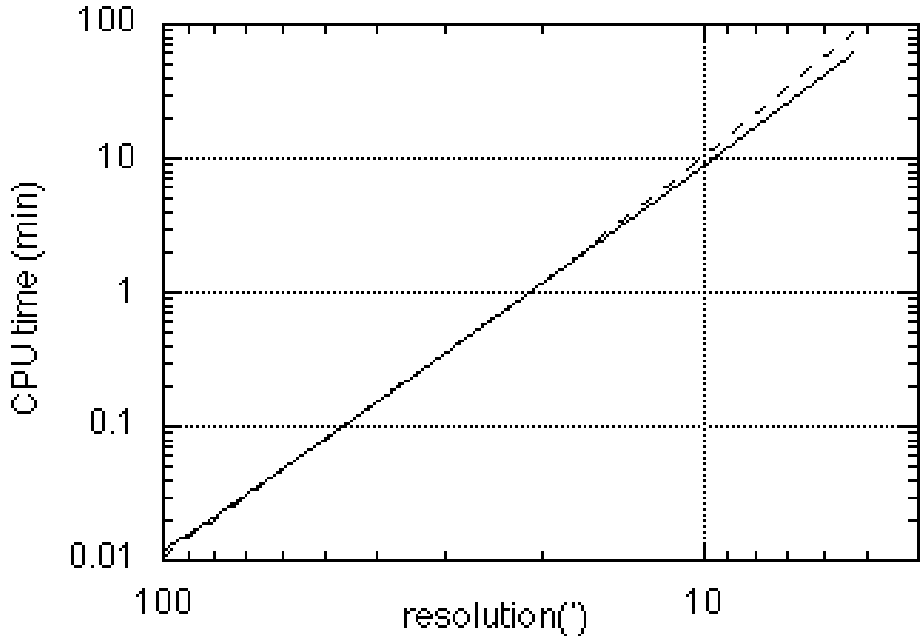

Figure 2: The CPU time needed, on a DEC 1000, to generate a full sky map (solid line) or to invert a map to generate the full set of $a_{\ell m}$'s (dotted line) as a function of the sampling of an Equidistant Cylindrical Projection of the sky.

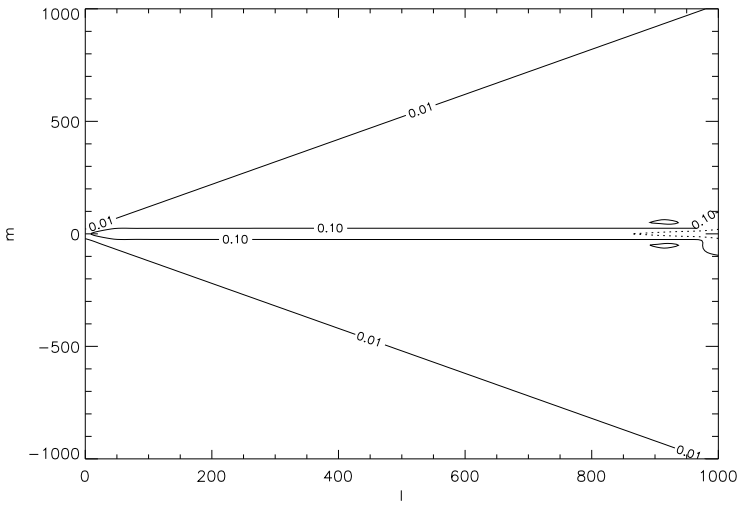

Figure 3: The percentage error between the recovered and the input, real part of the $a_{\ell m}$'s. The labels indicate the 0.01% and the 0.1% isolevel, respectively. Only in a very small portion of the $\ell - m$ plane the error is larger than 10% (dashed line).

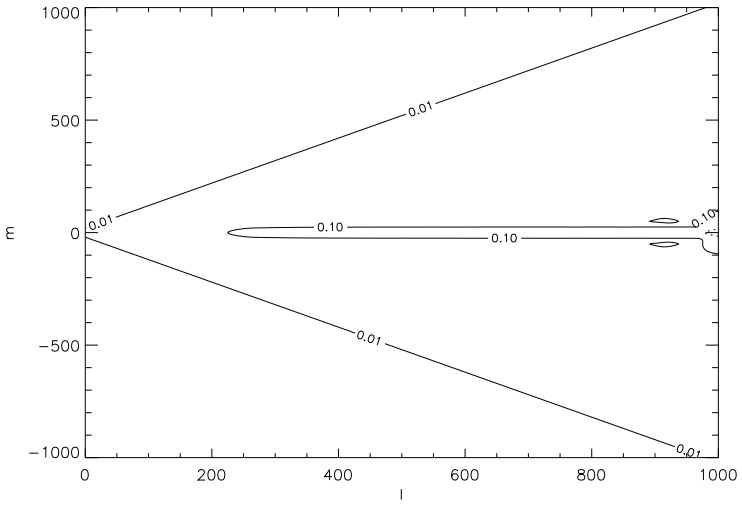

Figure 4: Same as in Fig.3, but for the imaginary part of the $a_{\ell m}$'s.

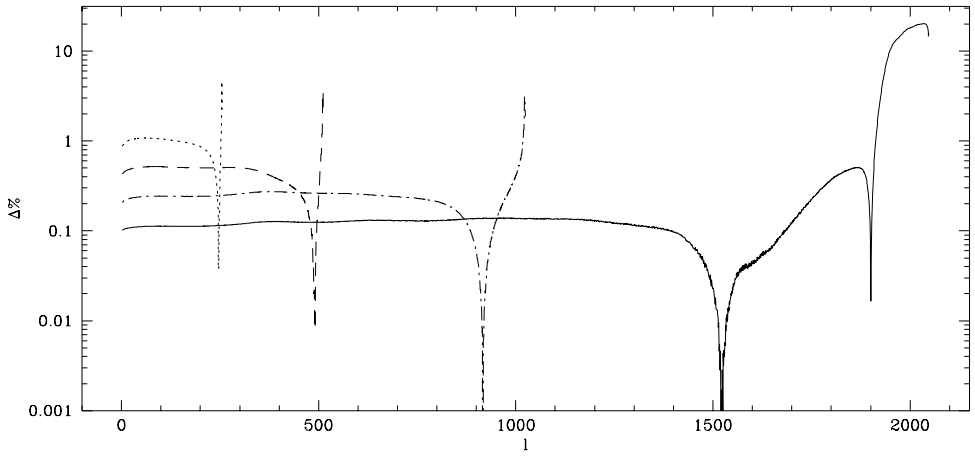

Figure 5: The percentage error between the recovered and the input spectral coefficients C_ℓ's as a function of ℓ for different resolutions of the Equidistant Cylindrical Projection of the CMB anisotropy pattern. Dotted, dashed, dot-dashed and continous lines refer to map resolution of $\simeq 40'$ ($\ell_{max} = 256$), $\simeq 20'$ ($\ell_{max} = 512$), $\simeq 10'$ ($\ell_{max} = 1024$), $\simeq 5'$ ($\ell_{max} = 2048$), respectively.

Figure 6: A realization of the CMB anisotropy pattern in a standard Cold Dark Matter model in the Equidistant Cylindrical (panel a) and in the Equal Area (panel b) Projections.

This figure "fig6.jpg" is available in "jpg" format from:

http://arXiv.org/ps/astro-ph/9703084v1